Earth and Planetary Science Letters 396 (2014) 46–55

Contents lists available at ScienceDirect

Earth and Planetary Science Letters

www.elsevier.com/locate/epsl

An analogue study of the influence of solidification on the advance and surface thermal signature of lava flows

F. Garel [a,b,c,*], E. Kaminski [a], S. Tait [a], A. Limare [a]

[a] Institut de Physique du Globe de Paris, Sorbonne Paris Cité, Univ. Paris Diderot, UMR CNRS 7154, 1 rue Jussieu, 75005 Paris, France
[b] School of Earth and Ocean Sciences, Cardiff University, Cardiff CF10 3YE, United Kingdom
[c] Department of Earth Science and Engineering, Imperial College London, London SW7 2AZ, United Kingdom

ARTICLE INFO

Article history:
Received 9 September 2013
Received in revised form 17 March 2014
Accepted 28 March 2014
Available online xxxx
Editor: T. Elliott

Keywords:
lava flows
analogue experiments
solidification during emplacement
thermal remote-sensing

ABSTRACT

The prediction of lava flow advance and velocity is crucial during an effusive volcanic crisis. The effusion rate is a key control of lava dynamics, and proxies have been developed to estimate it in near real-time. The thermal proxy in predominant use links the satellite-measured thermal radiated power to the effusion rate. It lacks however a robust physical basis to allow time-dependent modeling. We investigate here through analogue experiments the coupling between the spreading of a solidifying flow and its surface thermal signal. We extract a first order behavior from experimental results obtained using polyethylene glycol (PEG) wax, that solidifies abruptly during cooling. We find that the flow advance is discontinuous, with relatively low supply rates yielding long stagnation phases and compound flows. Flows with higher supply rates are less sensitive to solidification and display a spreading behavior closer to that of purely viscous currents. The total power radiated from the upper surface also grows by stages, but the signal radiated by the hottest and liquid part of the flow reaches a quasi-steady state after some time. This plateau value scales around half of the theoretical prediction of a model developed previously for the spreading and cooling of isoviscous gravity currents. The corrected scaling yields satisfying estimates of the effusion rate from the total radiated power measured on a range of basaltic lava flows. We conclude that a gross estimate of the supply rate of solidifying flows can be retrieved from thermal remote-sensing, but the predictions of lava advance as a function of effusion rate appears a more difficult task due to chaotic emplacement of solidifying flows.

1. Introduction

A major concern during an effusive volcanic eruption is how far and how fast lava will flow before it stops advancing. The real-time estimate of lava flow path and velocity is particularly important for volcanoes whose vicinity is inhabited. For example recent and historical lava flows have threatened towns and tourist facilities at Mt. Etna in Sicily (Barberi et al., 2003; Behncke et al., 2008). Another famous example in Italy is Mt. Vesuvius, whose flanks are densely populated in some places, and which has a long prior history of very regular effusive activity (Scandone et al., 1993) although it has not been active since 1944. For these two volcanoes, well-equipped observatories have been established to manage volcanic hazard. Another very important and topical example is that of Mt. Nyiragongo (Democratic Republic of Congo), whose lava flows have threatened, and in some phases actually invaded, the 400,000-inhabitant nearby city of Goma – 1977 and 2002 eruptions (Tazieff, 1977; Komorowski et al., 2002–2003). Although a volcanologic observatory does exist at Goma, it is not well-equipped, and has experienced severe operational restrictions during eruptive crises because of political unrest. In such circumstances, the evaluation of forthcoming hazard mainly relies on remote-sensing technologies. These techniques can also be useful in the case of an unusually large volcanic event, of which a recent example is the 2007 eruption of Piton de la Fournaise, Reunion Island (Staudacher et al., 2009) and during which even an advanced observatory can be stretched, with a limited ability to cover and monitor the whole lava flow field and its most hazardous, active parts. In general, the larger the event, the more appropriate and crucial becomes the use of remote sensing.

The final length of a lava flow is known to be strongly influenced by the effusion rate (e.g., Walker, 1973; Harris and Rowland, 2009). However, this conclusion has been reached based only on mean average effusion rates computed from *a posteriori* evaluations of the volume and duration of an eruption. Estimating effusion

* Corresponding author at: School of Earth and Ocean Sciences, Cardiff University, Cardiff CF10 3YE, United Kingdom. Tel.: +44 29 2087 5751.
E-mail address: GarelF@cardiff.ac.uk (F. Garel).

http://dx.doi.org/10.1016/j.epsl.2014.03.061
0012-821X/

rate in near real-time, though crucial for operational hazard assessment, is not yet fully operational. This measurement cannot easily be obtained via static ground-based technology since the location of the eruptive vents is not easily foreseeable and continuous visual monitoring requires important human and technical resources. Thus, simultaneous measurements of flow advance and lava flow rate remain very scarce for the moment (Naranjo et al., 1992; Coltelli et al., 2007). The difficulties of performing direct measurements have led to various attempts to develop proxies that might indirectly give access to effusion rates or their variations, such as tremor amplitudes (Battaglia et al., 2005), SO_2 output rates (Allard et al., 1994; Sutton et al., 2003) or surface thermal signal (e.g., Harris et al., 2007). However, a majority of such proxies are mainly empirical, and it remains difficult to assess their ability to provide robust quantitative estimates of effusion rates.

Of the methods cited above, the use of satellite measurements of radiated thermal power appears as the most flexible and promising at the moment. In particular, the thermal proxy of Harris and co-workers (e.g., Harris et al., 1997, 2007; Wright et al., 2001) is widely applied, underscoring the appeal of this approach. This thermal proxy originally relied on a model established for lava flows after they have stopped avancing (Pieri and Baloga, 1986). It was later formulated as a time-independent heat budget of a lava flow, where the heat sources (heat advection within the flow and crystallization) are balanced by the heat loss at the surface of the flow (Harris et al., 1998). The effusion rate Q is calculated as

$$Q = \frac{F_{tot}}{\rho(C_p \Delta T + \Phi c_L)}, \quad (1)$$

where F_{tot} is the total heat loss at the surface of the flow, in Watts, ρ, C_p, Φ and c_L are the lava density, specific heat, crystal content and latent heat of crystallisation, respectively, and ΔT is the temperature difference between the lava temperature at the vent and at the lava flow front. Several assumptions underlying this proxy have been criticized (Dragoni and Tallarico, 2009; Harris and Baloga, 2009). In particular, Eq. (1) does not take into account the fluid dynamics of the moving lava flow, hence cannot provide a consistent time-evolution of the surface thermal signal related to flow advance. A fluid mechanics investigation is necessary to understand the coupling between flow advance and cooling.

The advance of simple viscous gravity currents was studied first as a function of the supply rate and the (constant) fluid viscosity by Huppert (1982), who provided elegant scaling laws allowing a first-order interpretation of field observations on the spreading of lava bodies (Huppert et al., 1982). Currents with complex rheologies were investigated later (e.g., Stasiuk et al., 1993; Bercovici, 1994; Bercovici and Lin, 1996; Griffiths, 2000), with a main focus on the advance and surface morphologies of solidifying flows in analogue experiments using wax material (e.g., Fink and Griffiths, 1990, 1992; Blake and Bruno, 2000; Lyman and Kerr, 2006; Cashman et al., 2006; Robertson and Kerr, 2012). The supply rate and the cooling efficiency were shown to influence the flow regime and the rate of flow advance (Hallworth et al., 1987; Fink and Griffiths, 1990; Stasiuk et al., 1993). However, in these experimental works the flows were extruded underwater, hence their results cannot be used to investigate the thermal structure of the upper surface of the flows, leaving open the question of the relationship between the supply rate and the thermal power radiated by the flow.

We have started to investigate experimentally the relationship between supply rate and surface thermal signal for sub aerial viscous gravity currents (Garel et al., 2012), and we developed a model for the simultaneous cooling and spreading of an isoviscous gravity current. We showed that, as a function of the supply rate and of the fluid viscosity, a thermal steady state was established after a transient stage controlled by vertical heat conduction in the flow. Furthermore, we demonstrated that the thermal power radiated at steady state was indeed proportional to the effusion rate. We also used this theoretical model to investigate explicitly the surface heat transfer processes at the surface of the flow, taking into account different magnitudes of cooling by radiation or wind-induced convection (Garel et al., 2013).

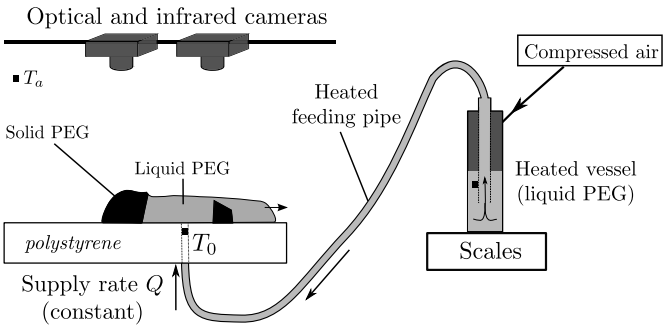

Fig. 1. Sketch of the experimental set-up. The source vessel and the feeding pipe are heated above PEG solidification temperature, by heating mats and a heating coil, respectively. Thermocouples (black squares) are placed in the vessel, in the air (T_a) and at the end of the pipe (T_0). The polystyrene support plate minimizes the basal heat loss, and is covered with a thin, easy-to-wash teflon film. The parameters of the performed experiments are given in Table 1.

An important limitation of this model is that temperature does not influence the flow rheology in isoviscous currents. To go beyond that limit, here we investigate the feedback of cooling on the flow dynamics with a set of analogue experiments using solidifying wax material. We focus on the evolution of the area and surface thermal signal of the currents, and use the experimental results to discuss the implications for the use of a thermal proxy for the effusion rate of lava flows.

2. Analogue material and experimental set-up

We study the spreading of hot solidifying wax material in the air in order to carry out remote infrared measurements of the flow surface temperatures. The fluid is the poly-ethylene glycol (PEG) P3515 of Sigma-Aldrich, with a melting point around 38 °C, similar to the one used in Hallworth et al. (1987). This PEG is different from the more commonly used PEG 600, that solidifies around 18 °C (Fink and Griffiths, 1990; Soule and Cashman, 2004). The viscosity of PEG P3515 was measured as a function of temperature with a Thermo-Haake rheometer using a cone-plate geometry. A viscosity jump of almost 6 orders of magnitude occurs around 37 °C at the transition between liquid and solid states. Details of the PEG physical properties are given in the supplementary material.

Fig. 1 presents a sketch of the experimental set-up. Liquid PEG, dyed green, is supplied at a rate Q (driven by a constant air overpressure in a supply vessel) and at a given temperature. Both parameters are constant during an experiment, and vary from one experiment to another (Table 1). The area covered by the current is measured on pictures taken from above, and its thermal structure (surface temperatures) is imaged with an infrared camera (FLIR SC645). The power (in Watts) radiated by the flow is calculated from the temperature measurements.

3. Emplacement of solidifying flows

3.1. Qualitative description of the spreading

Fig. 2 presents the evolution of the spreading liquid and solid PEG during experiment P302 ($T_0 = 46$ °C, $Q = 0.15$ cm^3/s), with coupled visible and infrared images. The PEG, injected in the liquid

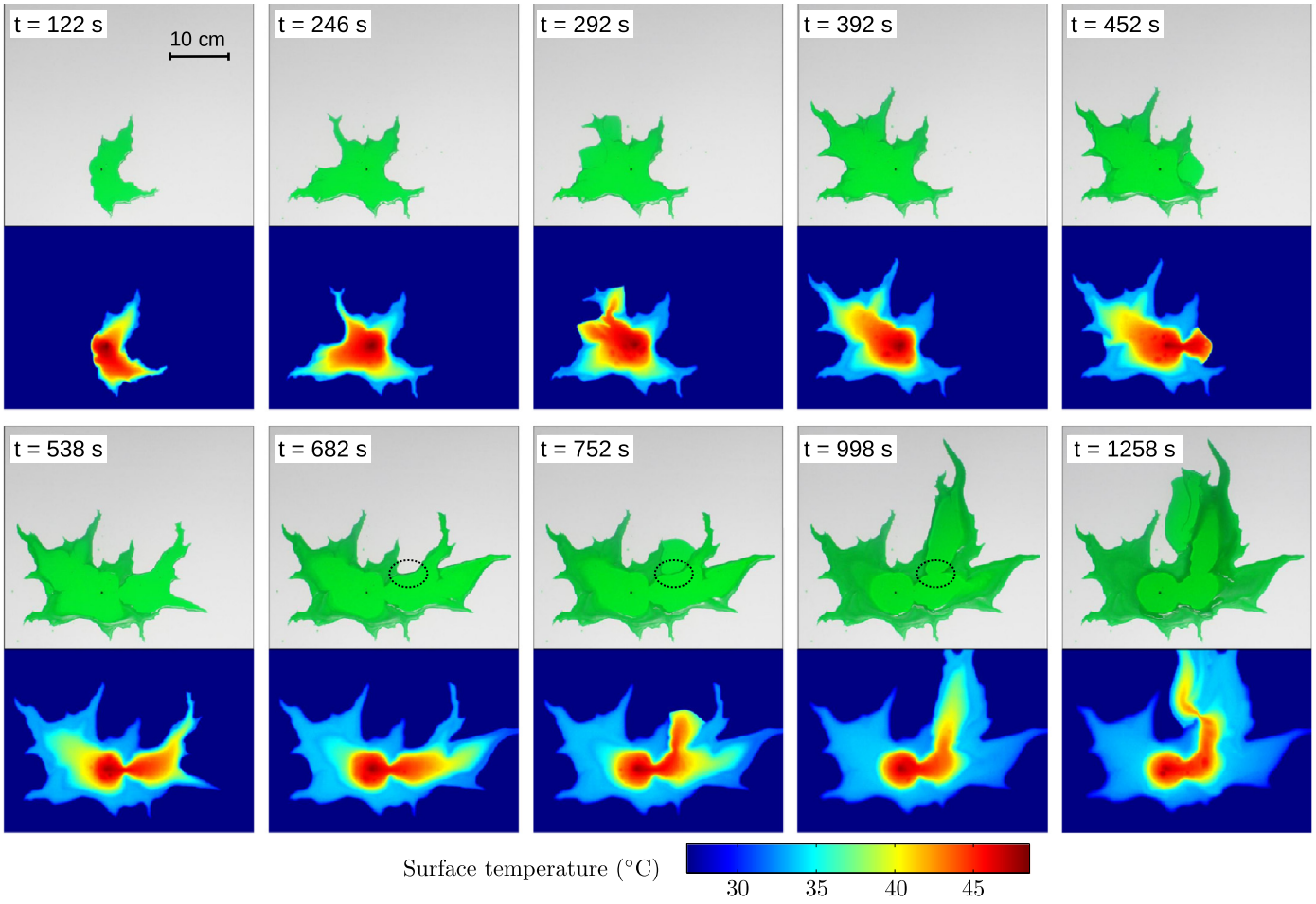

Fig. 2. Series of visible (top) and infrared (bottom) images taken during experiment P302 (source temperature T_0 of 46 °C and supply rate Q of 0.15 $cm^3\,s^{-1}$). The PEG is transparent green in its liquid state and opaque, dark green when solidified. Overflows of hot, liquid PEG, leading to the emplacement of "tongues" or lobes, are observed at 292, 452, 752 and 1258 s. The dashed circle between 682 and 998 s marks a region where solid material is thermally eroded by the overlying hot liquid. Surface tension may influence the tip flow morphology. The dynamic evolution is shown in the Supplementary Video. (For interpretation of the references to color in this figure legend, the reader is referred to the web version of this article.)

Table 1
Parameters of the experiments.

Experiment	Q ($cm^3\,s^{-1}$)	Source temperature T_0 (±1 °C)	Duration (min)
P202	0.14	43	20
P301	0.26	46	18
P302	0.15	46	22
P303	0.14	46	16
P401	0.55	46	10
P402	0.26	47	14
P403	0.27	47	8
P501	0.24	43	14
P502	0.40	44	12

Note: The ambient temperature T_a is 21 °C for all the experiments.

state, loses heat while moving away from the source and eventually completely freezes. The solidified material then acts as a barrier for newly injected fluid, leading to flow channelization between solid levees. Continuous injection of liquid PEG yields local overflowing above the solid barriers, with liquid spreading onto the plate before solidification occurs at the front.

A permanent pool of hot liquid PEG, which feeds distal overflows, is observed around the source throughout all the experiments. The PEG solidifies from the surface of the flow, and can remain liquid underneath the crust for several hours after the injection has stopped. Thermal erosion of the solid wax beneath hot liquid flow was sometimes observed (e.g., Fig. 2 between 682 and 998 s). In addition to solidification, flow advance in a given direction was sometimes limited by drainage in favor of other liquid overflows. We observed that liquid PEG P3515 is never able to break through the crust of wax, which precludes crust folding or liquid break-outs as was observed in underwater PEG 600 experiments (Fink and Griffiths, 1990; Blake and Bruno, 2000; Griffiths et al., 2003).

Because of overflows and levees, the solidifying PEG flow rapidly deviates from radial symmetry that characterizes the flow of an isoviscous fluid (Huppert, 1982; Garel et al., 2012), and we use the evolution of the current area with time to quantify the emplacement dynamics. As presented for experiment P302 in Fig. 3, the area of the current initially grows linearly with time (here until about 220 s) as expected for an isoviscous gravity current (Huppert, 1982). The slope of this graph is inversely proportional to the square root of viscosity in the isoviscous case (Huppert, 1982). Hence one can define an "apparent current viscosity" corresponding to the initial rate of flow advance, which, as one would expect, is larger than the viscosity of liquid PEG (here 2.6 vs. 0.15 Pa s) because of flow front solidification.

After its initial linear increase, the area continues to grow, but by stages, even though the injection of hot liquid PEG is continuous at the source (Fig. 3). The stagnation stages, during which the area increases not at all or very little, correspond to a rise

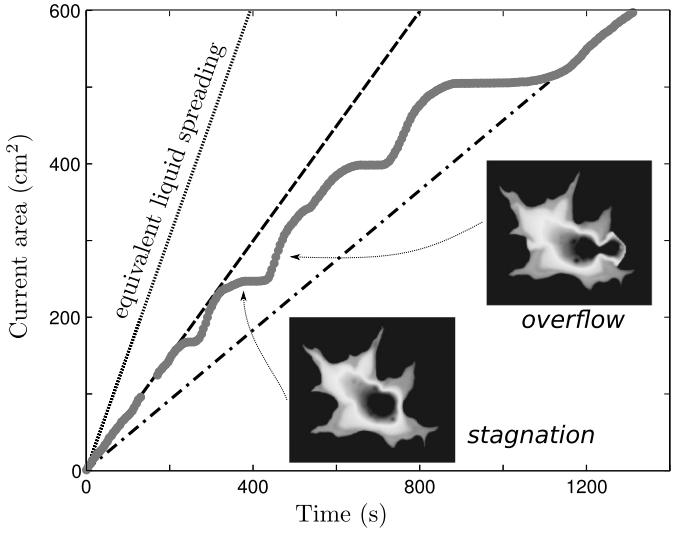

Fig. 3. Evolution of the current total area during experiment P302 (gray dots). The thin dashed line, dashed line and dash-dotted line indicate the spreading rate of a viscous gravity current with a viscosity 0.15 (liquid PEG), 2.6 (initial spreading) and 18.5 Pa s (final spreading). The insets show infrared images of successive stagnation and overflow phases (see Fig. 2 for length and temperature scales).

of level in the liquid pool around the source until the next overflow over its solid barriers occurs, followed by a fast-spreading episode. Similar discontinuous spreading was also observed for underwater PEG 600 wax flows with low supply rates (Hallworth et al., 1987) or with high cooling rates (Fink and Griffiths, 1990; Blake and Bruno, 2000). The duration of the stagnation phases increased during the course of an experiment (Fig. 3), yielding a decrease of the mean spreading rate of the current (hence a corresponding increase in the current thickness and in the apparent flow viscosity). The advance of the current is thus progressively slowed more and more efficiently by solidification. Overflows could be categorized as either volume- or cooling-limited whether they stopped because liquid material was drained by another overflow or because of solidification at the flow boundaries, by analogy with field observations on lava flows (Guest et al., 1987).

3.2. Influence of the supply rate on flow regimes

Fig. 4a compares the spreading rate for experiments P303 and P401, the latter having a supply rate four times larger than the former (Table 1). The mean spreading rate of the current increases with increasing supply rate, as for a viscous gravity current (Huppert, 1982).

The stagnation phases are clearly identified in experiments with a low supply rate (e.g., P303), whereas for higher supply rates (e.g., P401), the curves rather display "kinks" in the spreading rate, i.e. the increase of area is sometimes slowed down but never stops. The higher the supply rate, the closer the observed current spreading is to that of a viscous current of liquid PEG, a conclusion that was also drawn from underwater PEG experiments by Hallworth et al. (1987), Fink and Griffiths (1990), Blake and Bruno (2000). The area increase between two stagnation phases appears larger for a higher supply rate (Fig. 4a), corresponding to either larger or more frequent overflows. Since larger liquid volumes cool more slowly, and advance faster than ones with small volume (Huppert, 1982), the restraining effect of solidification on flow emplacement decreases with increasing supply rate. This raises the question of how to quantify best the behavior of currents which undergo large rheologic changes as they spread, a point that we discuss in Section 5.2.

3.3. Variability of spreading rates for comparable supply rates

In the case of an isoviscous fluid, the spreading rate is fully determined by the flow supply rate for given density and viscosity of the liquid (Huppert, 1982). In the present case, the rate of spreading is also controlled by the relative durations of stagnation phases and overflows, i.e. by the cooling efficiency. Experiments P202, P302 and P303, which have similar supply rates, display different morphologies and spreading rates (Fig. 4b). This variability is related to the variable shape of the PEG flow, which can exhibit fingered expansions (experiment P302), or meanders (experiment P202), that will in turn control the duration of the stagnation and flowing phases. Although solidification can produce discontinuous flow advance (experiment P302), it can also produce solid levees that will maintain a quasi-continuous spreading rate (experiment P202). The flow areas and morphologies, although similar, are not exactly reproducible for given conditions, because the solidification pattern causes somewhat random directions of flow advance. Hence the flow area cannot be predicted with high accuracy from the supply rate only.

For the same supply rate, the discrepancy between flow areas of experiment P303 and P202 can reach up to 30% (Fig. 4b). The spreading during the overflows in experiments P303 and P302 are very similar: notwithstanding the initial differences in spreading, the durations and slopes of later overflow stages match very well. This suggests that comparable supply rates can yield comparable volumes of liquid material available for overflows. We discuss in Section 5.2 the implications of these experimental results for volcanic hazard. We now investigate how we can use the thermal signal to constrain the source conditions, even though the spreading dynamics cannot be modeled using only the supply rate, because of the haphazard local variations in rheology.

4. Surface thermal signal of experimental solidifying flows

Even though we observe some variability in the current plan-view shape and spreading dynamics, the supply rate remains a first-order control parameter for flow advance. It is therefore still necessary to study if and how we can infer it from the surface thermal signal, i.e. the total thermal power radiated over the surface of the flows (in Watts), using the performed experiments.

4.1. Total radiated power

The integrated surface thermal signal (radiated power) is analogous to that which can be retrieved from lava flow thermal remote-sensing. The power radiated by the current is defined as

$$\phi_{rad} = \iint \varepsilon\sigma\left(T_{top}^4 - T_a^4\right) \mathrm{d}A, \tag{2}$$

with ε the emissivity, σ the Stefan–Boltzmann constant, T_{top} the surface temperature and T_a the ambient temperature. Fig. 5 presents the evolution of ϕ_{rad} during experiment P302. The step-like evolution is related to the discontinuous spreading rate of the current. The total radiated power can be viewed as the sum of two signals: (i) a thermal signal coming from the "inactive" old regions topped with solidified PEG, and (ii) a signal radiated by the exposed, flowing liquid (the hottest part of the flow – the "active" flow).

During stagnation phases, net cooling occurs (resulting in a small decrease in the radiated power), whereas overflows are associated with bursts in the radiant power since they create new hot current areas. On the time-scale of our experiments, the total radiant power did not reach a steady state, in contrast to the case of viscous currents of silicone oil investigated in our previous study (Garel et al., 2012). Fig. 6a shows the global consistency between

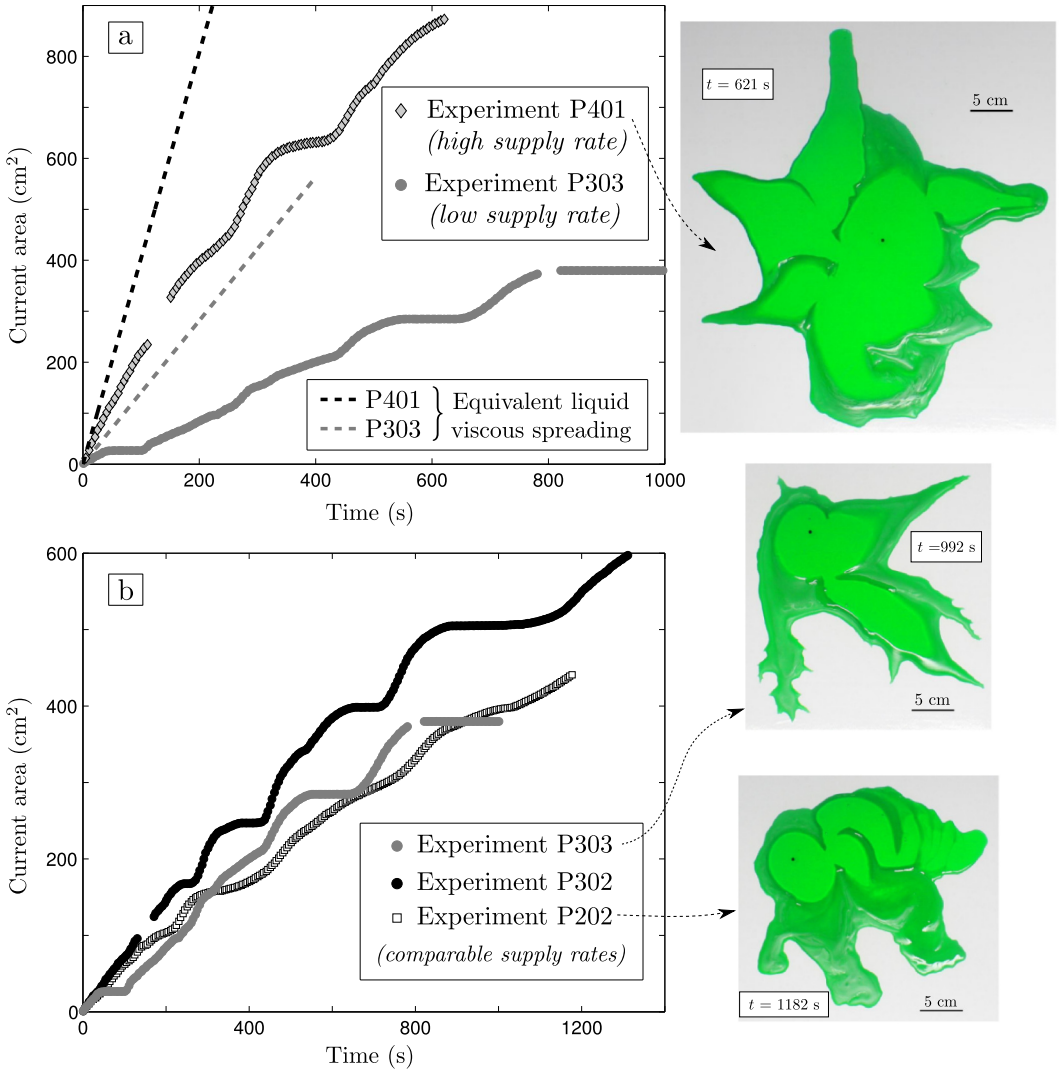

Fig. 4. (a) Evolution of the current area for experiment P303 ($Q = 0.14$ cm^3 s^{-1}) and P401 ($Q = 0.55$ cm^3 s^{-1}). The dashed lines indicate the equivalent spreading of liquid PEG for the same supply rates. The images on the right show the flow morphologies (same scale). (b) Spreading rates of flow emplacement during experiments P202, P302 and P303 (comparable supply rates, see Table 1).

the evolution of the area and of the radiated power. We observe at first order a smooth, monotonic increase of the radiated power and current area, and the discontinuous pattern of both spreading and thermal signal (Figs. 3 and 5) is "erased". The signature of the supply rate can thus be seen more easily, and is not hidden by the transition between overflow and stagnation phases: we see clearly on Fig. 6a that a high supply rate maintains higher surface temperatures, and over a longer time/larger area than small supply rates. We note as well that during the course of an experiment, the mean surface temperature of the material decreased with time (i.e. the curves tend to get closer to the lowest isotherm, e.g. experiment P502). Under a constant input rate, an area at hot temperature with a relatively constant spatial extent is maintained. However, cooling and solidified material is constantly accumulated through time, and exhibits a thermal signature long after its emplacement. Hence, for a constant input rate, the contribution of the colder parts of the flow to the bulk radiated power will become more and more important with time.

4.2. Thermal signal of active vs. inactive flow regions

Even though the current regions covered by solidified PEG may have ceased to advance, they still contribute to the total radiated power since they remain hotter than the ambient air. To relate the thermal power to the supply rate, we introduce a temperature threshold in order to discriminate the contributions of active and inactive flow regions. This enables us to define a threshold power, radiated by the part of the flow whose surface temperature exceeds the corresponding threshold temperature T_{thr}. Fig. 5 presents the evolution of these "threshold" radiated powers, whose values decrease as the temperature threshold increases. For a threshold temperature greater than or equal to 37 °C (the nominal solidification temperature of PEG), the threshold radiated power presents an initial transient increase followed by a plateau-like stage, which mimics the evolution obtained for an isoviscous hot gravity current by Garel et al. (2012).

The quasi-steady stage defined using high threshold temperatures is punctuated with bursts in the radiated power, corresponding to overflows of liquid material above the solid barriers (Fig. 5). The finite durations of these bursts confirm the previous observation that a liquid overflow has a finite lifetime: it ineluctably cools down as it spreads, eventually solidifies and stops advancing. The amplitude and duration of these bursts, as well as the duration of the transient stage of increasing radiated power, decrease with increasing threshold surface temperature. The hotter regions are

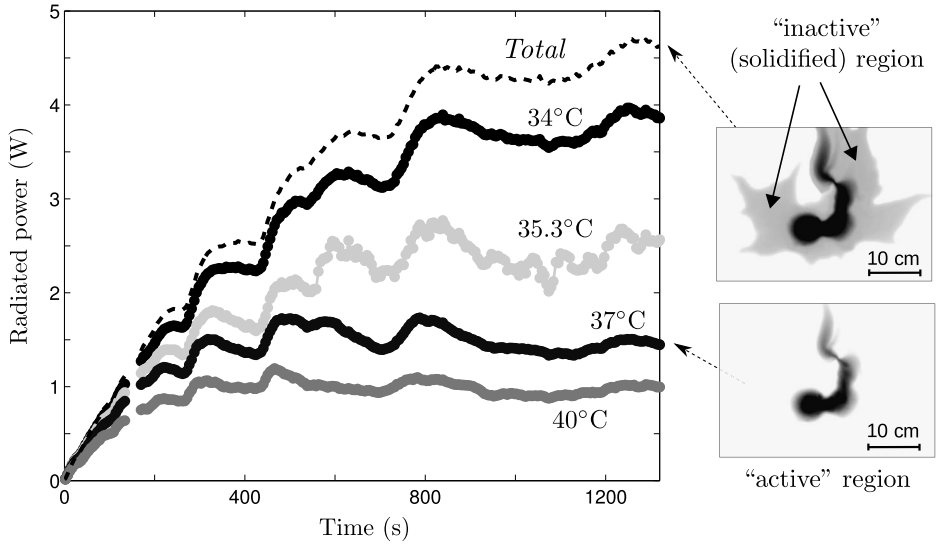

Fig. 5. Temporal evolution of the power radiated by the emplaced PEG during experiment P302. The total radiated power is indicated by the black dashed line, and the subsequent plots are the powers radiated by regions of the current with surface temperature greater than a given threshold. Note that the current exceeds the field of view of the infrared image around 800 s (see Fig. 2), hence powers radiated by low-temperature regions are underestimated after that time. The images show the contour of the region with a surface temperature greater than the threshold.

indeed mainly located in the stagnant pool, and less affected by the overflow episodes.

The stability of the hottest regions of the flow can also be illustrated by looking at the evolution of the "threshold" areas (i.e. the current area with a surface temperature higher than a given value) as a function of the chosen surface temperature threshold (Fig. 6b). At the beginning of the experiment, we observe a quasi-constant area as a function of the temperature threshold, which indicates that the current is very hot. As time goes by, we observe a growing discrepancy between threshold areas for low temperatures and those for higher temperatures. Threshold areas for temperatures lower than 35 °C are continuously increasing whereas for surface temperatures higher than 37 °C the area becomes stationary after an initial transient. This evolution is similar to that observed for the threshold radiated power on Fig. 5: the area of the liquid regions becomes constant for a constant supply rate.

In order to compare the constant supply rate and the thermal signal, it is necessary to retrieve a steady value for the "active" radiated power. We choose the threshold temperature of 40 °C in order to limit the influence of the thermal bursts. Fig. 7 presents the relationship between these "active" radiated powers and the supply rates for all the performed experiments. The intensity of the "active" surface thermal signal increases with increasing supply rate, as was found for the case of isoviscous gravity currents (Garel et al., 2012). The issue is then to derive a quantitative relationship between the two parameters, since the ultimate goal is the extrapolation of the experimental results to thermal remote sensing of lava flows, which also exhibit a temperature dependence of rheology albeit more complicated than PEG.

4.3. Definition of a quantitative thermal proxy

We have developed in a previous paper a model for the cooling of an isoviscous gravity current, in which the thermal steady state resulted from a balance between heat advection within the current and surface heat loss (Garel et al., 2012). This model is not directly applicable to the solidifying PEG flows in which we have seen that solid levees can temporarily confine liquid flow, and (somewhat randomly) orientate flow outbursts. However, for the hottest part of the current (in which PEG is a viscous liquid), the power radiated reached a steady state after a period of transient increase, as for an isoviscous fluid. This favors the use of the isoviscous theoretical model to relate the steady threshold radiated powers with the supply rate. Fig. 8 shows the comparison between data and model predictions based on the experimental parameters (supply rate, source and ambient temperatures) from Table 1, the material parameters given in the supplementary material, and using the liquid PEG viscosity (about 0.15 Pa s). Despite the complexity of the PEG emplacements and the issue of latent heat release, the theoretical predictions are proportional to the experimental results, showing that the isoviscous scaling is able to provide a robust estimate of the supply rate. This match is likely to reflect a relationship between the liquid pool area and the supply rate.

The measured power is about half that predicted by the isoviscous model of Garel et al. (2012). This can be explained by a larger effective viscosity of the spreading PEG than the nominal value of the liquid PEG. This is confirmed by the observation of the flow thickness in the experiments, which is around 3 mm whereas the viscous height predicted using the liquid viscosity would be around 1 mm. The higher effective viscosity of the flowing PEG is confirmed by a higher duration of the transient increase of the active radiated power before it reaches its plateau value compared to the isoviscous model predictions (Garel et al., 2012), e.g. for experiment P302 around 200–300 s (see Fig. 5) instead of the predicted 150 s.

5. Discussion

5.1. Thermal remote-sensing of lava flows

The experiments have shown that the global increase of radiated power with effusion rate is still valid for a solidifying material. This trend has also been observed for basaltic lava flows by Coppola et al. (2013), as shown in Fig. 9. There is however a large difference between the thermal signal of basaltic and acidic lavas for the same effusion rate, which can be explained by the long transient stage predicted by Garel et al. (2012) for very viscous lavas. As only basaltic lavas are likely to reach a steady state thermal regime, we compare the data on basaltic lava flows with the nominal prediction of the theoretical model of Garel et al. (2012), as well as with the scaling of Fig. 8. Fig. 9 shows that both trends account fairly well for the field observations. This comparison suggests that solidification does not invalidate the use of

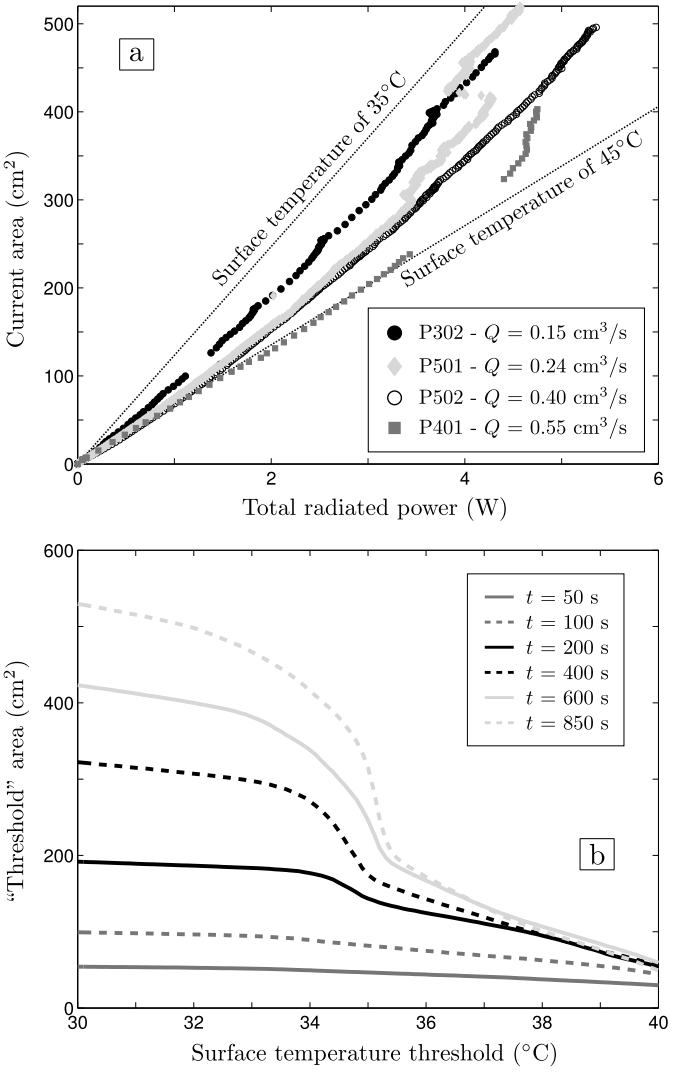

Fig. 6. (a) Current area as a function of the total radiated power for different experiments (see Table 1 for other experimental parameters). The dotted lines indicate the coupled evolution of radiated power and function of area for a constant surface temperature (either 35 or 45 °C). (b) Area of the current hotter than a given surface temperature threshold at different times during experiment P501. The emplaced PEG material remained in the field of view of the thermal infrared image during the whole experiment. The time at which the threshold area becomes constant increases with decreasing temperature threshold.

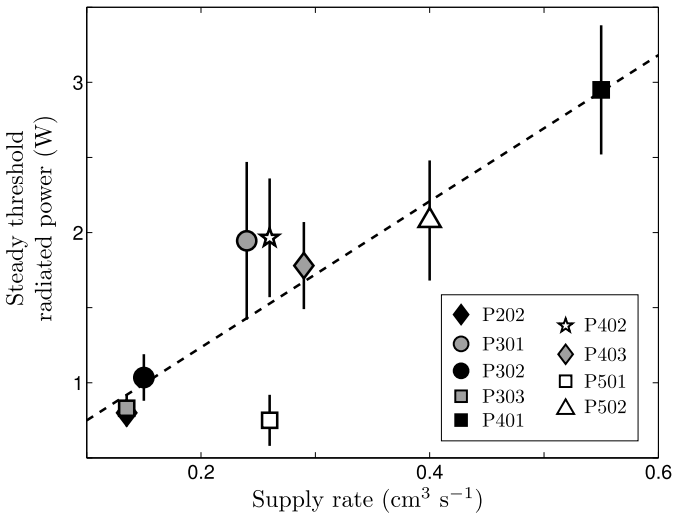

Fig. 7. Quasi-steady threshold radiated power as a function of supply rates for a threshold temperature of 40 °C. Note the discrepancy between experiment P501 and experiments P301, P402 and P403 that is probably due to the lower source temperature T_0 for P501 (see Table 1).

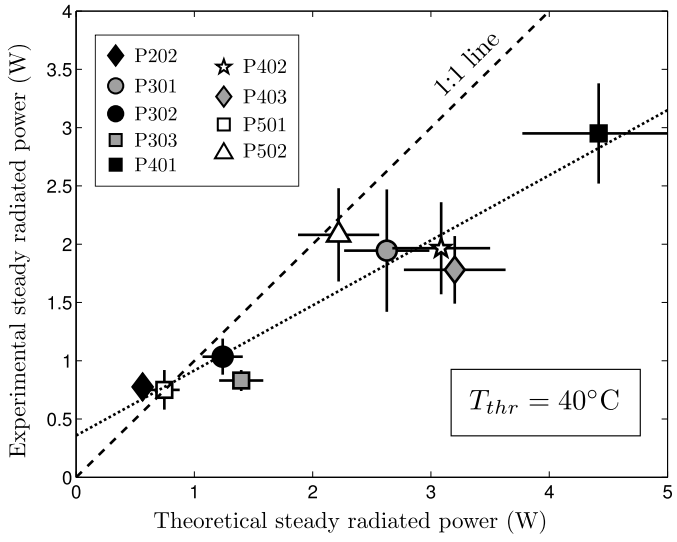

Fig. 8. Comparison between experimental and theoretical steady threshold radiated powers for a surface temperature threshold of 40 °C. The dotted line has a slope of 0.56 and the experimental radiated power at the origin is 0.36 W. The experimental uncertainties are related to the amplitude of the thermal bursts associated with overflows. The theoretical predictions are obtained from the isoviscous scaling (Garel et al., 2012), with theoretical errorbars accounting for a convective heat transfer coefficient λ varying between 1 and 3 W m^{-1} K^{-1} (free convection range).

the isoviscous thermal proxy for the effusion rate. This can be explained by the counterbalancing effects of an increase in apparent viscosity (increase in flow thickness, decrease in flow area and radiated signal), and latent heat of crystallization (decrease of cooling efficiency). The uncertainty on the effusion rate calculated from thermal data remains quite large, around 50%, due to uncertainties on the effective flow viscosity and variable efficiency of convective cooling at the flow surface (Garel et al., 2013).

The experimental results lead us to strike a note of additional caution concerning the use of thermal remote-sensing to estimate lava effusion rate. The time-dependence of the power radiated by a solidifying flow (initial transient increase, overflows yielding episodic thermal bursts) underlines the need for continuous and high-frequency thermal monitoring to detect dangerous overflows or sudden increases of volcanic activity. The comparison of radiated power and flow areas as a function of time (Fig. 6a) can be used to discriminate flow regimes, as done for the 2001 lava flow of Mt. Etna by Harris et al. (2010). Retrieving the temporal evolution of the area hotter than a certain threshold (similar to Fig. 6b) may also yield information about the thermal structure of the flow. This would be especially interesting to track tube systems, as well as lava break-outs, for which the melt underneath will eventually rupture the solidified crust (e.g., Calvari and Pinkerton, 1998; Applegarth et al., 2010). These systems are expected to display a weak radiated power and overall surface thermal signature (Realmuto et al., 1992), contrasting with their ability to supply bursts of very hot (fluid) lava, generating rapid spreading from the flow front (Calvari and Pinkerton, 1998; Harris and Rowland, 2009). Hence, high-frequency monitoring appears also crucial to survey the surface extent of the lava flow field and discriminate thermal structures.

The discrimination of active areas in lava flow fields using remote-sensing will however be less straightforward than in the experiments since satellite radiances are derived from Planck's law and integrated over a range of temperatures (Dozier, 1981).

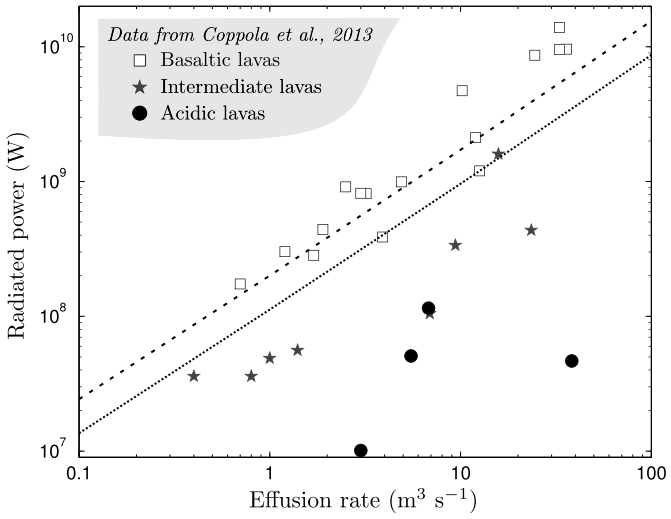

Fig. 9. Measured powers radiated by lava flows as a function of their effusion rate. The dashed line represents the nominal predictions for steady radiated powers of the isoviscous model (Garel et al., 2012), and the dotted line shows the scaling correction of 0.56 applied to these predictions, in agreement with Fig. 8. The lava flow data are from Coppola et al. (2013); basaltic and intermediate lavas having SiO_2 content lower or equal to 50% or 60%, respectively, and acidic lava higher than 60%. The theoretical predictions are made using the following parameters: emissivity 0.97, source temperature 1100 °C, ambient temperature 20 °C, viscosity 1000 Pa s, density 2300 kg m^{-3}, specific heat 1000 J kg^{-1} K^{-1}, thermal conductivity 3 W K^{-1} m^{-1} and convective heat transfer coefficient of 50 W m^{-2} K^{-1}.

Satellite sensors operating at low wavelengths are more sensitive to active lava features (Aries et al., 2001). The automatic detection of volcanic eruptions from space (Wright et al., 2004; Ferrucci et al., 2013) can also give some leads on how to combine satellite spectral radiances at different wavelengths to gain information about the surface temperature distribution.

5.2. Hazard of lava flow advance: input from modeling

Modeling lava emplacement is crucial for real-time mitigation during an effusive eruption, and for long-term hazard assessment in the volcano vicinity (e.g., Rowland et al., 2005; Vicari et al., 2007; Hérault et al., 2011). Both our and previous experiments have shown that the spreading of a solidifying material is often highly discontinuous, with alternations between phases of stagnation and phases of rapid flow advance: overflows in our experiments, break-outs and overflows in other underwater PEG experiments (Hallworth et al., 1987; Fink and Griffiths, 1990; Blake and Bruno, 2000) and break-outs in controlled lava pouring experiments (Syracuse project, personal communication of Einat Lev). Lava emplacement in nature can also exhibit these episodic features (Guest et al., 1987; Hon et al., 1994; James et al., 2012).

The analogue experiments show that the volume available for, and the frequency of overflows increase with the source supply rate. We observed the influence of supply rate on flow regime, concurring with the experimental results of Blake and Bruno (2000) and the analysis of lava flow advance of Castruccio et al. (2013). The previous attempts to quantify the effect of solidification derived either an effective viscosity (Stasiuk et al., 1993) or a yield strength for the flow (Griffiths and Fink, 1993). They cannot however fully predict the discontinuous and chaotic emplacement of solidifying flows, whose advance is not exactly reproducible (Hallworth et al., 1987).

Field observations of recent eruptions suggest that high effusion rates yield long lava flows, whereas low effusion rates lead to shorter flows and compound flow fields (Walker, 1973; Wadge, 1978; Guest et al., 1987; Harris and Rowland, 2009). On the larger scale of continental flood basalts, Self et al. (1996) and Thordarson and Self (1998) have reached the conclusion that compounds lava flows could slowly be emplaced over large areas during several years with a low cooling rate maintained during lava transport. The flow regime and thermal insulation therefore play a major role in setting the effective rheology of a lava flow.

The effusion rate plays a key role in lava emplacement, but, from the experimental results on solidifying flows, does not appear as a fully deterministic parameter. A scaling for the influence of effusion rate on lava length would be hard to derive since the transitions between stagnation, overflow and break-out phases are likely to depend on the local topography. Empirical scaling laws between effusion rate and final flow length have been derived on Mt. Etna based on historical eruptions (Calvari and Pinkerton, 1998). A future challenge is to use fast-computing models of lava flow advance – e.g. MAGFLOW (Vicari et al., 2007; Bilotta et al., 2012), or LavaSIM (Hidaka et al., 2005; Proietti et al., 2009) – to understand which effective rheology, maybe depending on the effusion rate, would reproduce best the advance of solidifying lava flows.

5.3. Other controls on lava flow advance and surface thermal signal

Our experiments investigated the cooling of a simple expanding, solidifying flow. Lava flows can however display different features that may affect (i) the relationship between radiated power and effusion rate, and (ii) the prediction of flow advance from effusion rate.

The horizontal support in the experiments allowed a spreading in multiple directions, whereas natural slope of volcanic flanks are expected to focus flow spreading downslope. Nevertheless, we still expect the local morphology (levees, crust) to play a role during lava outbreaks or overflow events, making the prediction of lava flow path difficult.

Surface thermal structure is, with flow area, the key factor determining the intensity of the power radiated by a lava flow. Our experiments exhibit a clear discrepancy between liquid, flowing material with high surface temperatures, and solidified material that has ceased to advance, similar to a flowing lava channel and its levees. The existence of solid crust on top of a moving flow would modify the flow cooling rate, and yield a radiated signal sensitive to the crust coverage and to the amount of hot melt exposed through the crust fractures (Crisp and Baloga, 1990; Wright et al., 2010). Flow velocity is likely to affect crust coverage, e.g. following a change in slope or in flow dimensions (Cashman et al., 2006).

The feedback of flow spreading on its rheology through crystallisation (Castruccio et al., 2010) and surface solidification (Griffiths and Fink, 1993; Castruccio et al., 2013) will determine the time- and length-scales of flow advance and associated surface thermal signal. Hence, changes in effusion rate, lava chemistry or crystal content during the course of an eruption should also affect the conversion of remote-sensing data to effusion rate.

6. Conclusion

We have carried out laboratory experiments using PEG wax as an analogue for lava, in order to investigate the links between the supply rate and the thermal power radiated from the flow surface. Both the dynamics of emplacement of the solidifying material and the temporal evolution of its surface thermal signal have been monitored. While experiments are performed with a constant supply rate, flow emplacement occurs by episodic liquid overflows above solid barriers. For a given supply rate, we observe a large variability of flow geometry and flow regimes. However, despite the complexity of flow emplacement, we showed that the supply rate of a solidifying flow could, at first order, be retrieved from

the surface thermal signal radiated by the hottest part of the flow, using a simple isoviscous theoretical model developed in Garel et al. (2012). The extrapolation of our results to natural cases shows that the radiated power indeed provides a first-order estimate of the effusion rate of basaltic lava flows. However, the uncertainty in this estimation is always significant (about 50%), because of the chaotic flow dynamics and of the variable convective cooling at the surface of the flow.

As a matter of fact, although the supply rate is the main control on the advance of a solidifying flow, our simple and controlled experiments display non-predictable flow emplacement and flow regimes for the same supply rate. Fast-computing models of lava advance on the actual volcano topography, as well as the compilation of historical data of lava flow emplacement, could help to better constrain the influence of effusion rate on the effective flow rheology. The coupling of such models to high frequency remote-sensing, as developed in the LAV@HAZARD framework (Ganci et al., 2012), appears as one of the most promising tools for the management of effusive volcanic hazard.

Acknowledgements

We thank two anonymous reviewers for useful comments on this manuscript, and are grateful to Tim Elliott for the editorial handling.

Appendix A. Supplementary material

Supplementary material related to this article can be found online at http://dx.doi.org/10.1016/j.epsl.2014.03.061.

References

Allard, P., Carbonnelle, J., Metrich, N., Loyer, H., Zettwoog, P., 1994. Sulphur output and magma degassing budget of Stromboli volcano. Nature 368, 326–330.
Applegarth, L., Pinkerton, H., James, M., Calvari, S., 2010. Lava flow superposition: the reactivation of flow units in compound 'a'ā flows. J. Volcanol. Geotherm. Res. 194, 100–106.
Aries, S., Harris, A., Rothery, D., 2001. Remote infrared detection of the cessation of volcanic eruptions. Geophys. Res. Lett. 28, 1803–1806.
Barberi, F., Brondi, F., Carapezza, M., Cavarra, L., Murgia, C., 2003. Earthen barriers to control lava flows in the 2001 eruption of Mt. Etna. J. Volcanol. Geotherm. Res. 123, 231–243.
Battaglia, J., Aki, K., Staudacher, T., 2005. Location of tremor sources and estimation of lava output using tremor source amplitude on the Piton de la Fournaise volcano: 2. Estimation of lava output. J. Volcanol. Geotherm. Res. 147, 291–308.
Behncke, B., Calvari, S., Giammanco, S., Neri, M., Pinkerton, H., 2008. Pyroclastic density currents resulting from the interaction of basaltic magma with hydrothermally altered rock: an example from the 2006 summit eruptions of Mount Etna, Italy. Bull. Volcanol. 70, 1249–1268.
Bercovici, D., 1994. A theoretical model of cooling viscous gravity currents with temperature-dependent viscosity. Geophys. Res. Lett. 21, 1177–1180.
Bercovici, D., Lin, J., 1996. A gravity current model of cooling mantle plume heads with temperature-dependent buoyancy and viscosity. J. Geophys. Res. 101, 3291–3309.
Bilotta, G., Cappello, A., Hérault, A., Vicari, A., Russo, G., Del Negro, C., 2012. Sensitivity analysis of the MAGFLOW Cellular Automaton model for lava flow simulation. Environ. Model. Softw. 35, 122–131.
Blake, S., Bruno, B.C., 2000. Modelling the emplacement of compound lava flows. Earth Planet. Sci. Lett. 184, 181–197.
Calvari, S., Pinkerton, H., 1998. Formation of lava tubes and extensive flow field during the 1991–1993 eruption of Mount Etna. J. Geophys. Res. 103, 27291–27301.
Cashman, K.V., Kerr, R.C., Griffiths, R.W., 2006. A laboratory model of surface crust formation and disruption on lava flows through non-uniform channels. Bull. Volcanol. 68, 753–770.
Castruccio, A., Rust, A., Sparks, R., 2010. Rheology and flow of crystal-bearing lavas: Insights from analogue gravity currents. Earth Planet. Sci. Lett. 297, 471–480.
Castruccio, A., Rust, A., Sparks, R., 2013. Evolution of crust- and core-dominated lava flows using scaling analysis. Bull. Volcanol. 75.
Coltelli, M., Proietti, C., Branca, S., Marsella, M., Andronico, D., Lodato, L., 2007. Analysis of the 2001 lava flow eruption of Mt. Etna from three-dimensional mapping. J. Geophys. Res. 112, F02029.
Coppola, D., Laiolo, M., Piscopo, D., Cigolini, C., 2013. Rheological control on the radiant density of active lava flows and domes. J. Volcanol. Geotherm. Res. 249, 39–48.
Crisp, J., Baloga, S., 1990. A model for lava flows with two thermal components. J. Geophys. Res., Solid Earth 1978–2012 (95), 1255–1270.
Dozier, J., 1981. A method for satellite identification of surface temperature fields of subpixel resolution. Remote Sens. Environ. 11, 221–229.
Dragoni, M., Tallarico, A., 2009. Assumptions in the evaluation of lava effusion rates from heat radiation. Geophys. Res. Lett. 36, L08302.
Ferrucci, F., Theys, N., Clarisse, L., Hirn, B., Laneve, G., Valks, P., Der Van A, R., Tait, S., Di Bartola, C., Brenot, H., 2013. Operational integration of spaceborne measurements of Lava discharge rates and Sulphur Dioxide concentrations for Global Volcano Monitoring. In: Wenzel, F., Zschau, J. (Eds.), Early Warning for Geological Disasters-Scientific Methods and Current Practice. Springer.
Fink, J., Griffiths, R., 1990. Radial spreading of viscous-gravity currents with solidifying crust. J. Fluid Mech. 221, 485–509.
Fink, J., Griffiths, R., 1992. A laboratory analog study of the surface morphology of lava flows extruded from point and line sources. J. Volcanol. Geotherm. Res. 54, 19–32.
Ganci, G., Vicari, A., Cappello, A., Del Negro, C., 2012. An emergent strategy for volcano hazard assessment: from thermal satellite monitoring to lava flow modeling. Remote Sens. Environ. 119, 197–207.
Garel, F., Kaminski, E., Tait, S., Limare, A., 2012. An experimental study of the surface thermal signature of hot subaerial isoviscous gravity currents: implications for thermal monitoring of lava flows and domes. J. Geophys. Res. 117, B02205.
Garel, F., Kaminski, E., Tait, S., Limare, A., 2013. The influence of wind on the estimation of lava effusion rate from thermal remote-sensing. J. Volcanol. Geotherm. Res. 264, 223–230. http://dx.doi.org/10.1016/j.jvolgeores.2013.08.006.
Griffiths, R., Fink, J., 1993. Effects of surface cooling on the spreading of lava flows and domes. J. Fluid Mech. 252, 667–702.
Griffiths, R., Kerr, R., Cashman, K., 2003. Patterns of solidification in channel flows with surface cooling. J. Fluid Mech. 496, 33–62.
Griffiths, R.W., 2000. The dynamics of lava flows. Annu. Rev. Fluid Mech. 32, 477–518.
Guest, J., Kilburn, C., Pinkerton, H., Duncan, A., 1987. The evolution of lava flowfields: observations of the 1981 and 1983 eruptions of Mount Etna, Sicily. Bull. Volcanol. 49, 527–540.
Hallworth, M.A., Huppert, H.E., Sparks, R.S.J., 1987. A laboratory simulation of basaltic lava flows. Mod. Geol. 11, 93–107.
Harris, A., Baloga, S., 2009. Lava discharge rates from satellite-measured heat flux. Geophys. Res. Lett. 36, L19302.
Harris, A., Blake, S., Rothery, D., Stevens, N., 1997. A chronology of the 1991 to 1993 Mount Etna eruption using advanced very high resolution radiometer data: implications for real-time thermal volcano monitoring. J. Geophys. Res. 102, 7985–8003.
Harris, A., Dehn, J., Calvari, S., 2007. Lava effusion rate definition and measurement: a review. Bull. Volcanol. 70, 1–22.
Harris, A., Favalli, M., Steffke, A., Fornaciai, A., Boschi, E., 2010. A relation between lava discharge rate, thermal insulation, and flow area set using lidar data. Geophys. Res. Lett. 37, L20308.
Harris, A., Flynn, L., Keszthelyi, L., Mouginis-Mark, P., Rowland, S., Resing, J., 1998. Calculation of lava effusion rates from Landsat TM data. Bull. Volcanol. 60, 52–71.
Harris, A., Rowland, S., 2009. Effusion rate controls on lava flow length and the role of heat loss: a review. In: Thordarson, T., Self, S., Larsen, G., Rowland, S.K., Hoskuldsson, A. (Eds.), Studies in Volcanology: The Legacy of George Walker. In: Special Publications of IAVCEI, pp. 33–51.
Hérault, A., Bilotta, G., Vicari, A., Rustico, E., Del Negro, C., 2011. Numerical simulation of lava flow using a GPU SPH model. Ann. Geophys. 54.
Hidaka, M., Goto, A., Umino, S., Fujita, E., 2005. VTFS project: development of the lava flow simulation code LavaSIM with a model for three-dimensional convection, spreading, and solidification. Geochem. Geophys. Geosyst. 6.
Hon, K., Kauahikaua, J., Denlinger, R., Mackay, K., 1994. Emplacement and inflation of pahoehoe sheet flows: observations and measurements of active lava flows on Kilauea Volcano, Hawaii. Geol. Soc. Am. Bull. 106, 351–370.
Huppert, H., 1982. Propagation of two-dimensional and axisymmetric viscous gravity currents over a rigid horizontal surface. J. Fluid Mech. 121, 43–58.
Huppert, H., Shepherd, J., Sigurdsson, H., Sparks, R., 1982. On lava dome growth, with application to the 1979 lava extrusion of the Soufriere of St. Vincent. J. Volcanol. Geotherm. Res. 14, 199–222.
James, M., Applegarth, L., Pinkerton, H., 2012. Lava channel roofing, overflows, breaches and switching: insights from the 2008–2009 eruption of Mt. Etna. Bull. Volcanol. 74, 107–117.
Komorowski, J., Tedesco, D., Kasereka, M., Allard, P., Papale, P., Vaselli, O., Durieux, J., Baxter, P., Halbwachs, M., Akumbe, M., et al., 2002–2003. The January 2002 flank eruption of Nyiragongo volcano (Democratic Republic of Congo): Chronology, evidence for a tectonic trigger, and impact of lava flows on the city of Goma. Acta Vulcanol. 14–15, 27–61.
Lyman, A., Kerr, R., 2006. Effect of surface solidification on the emplacement of lava flows on a slope. J. Geophys. Res. 111, B05206.

Naranjo, J., Sparks, R., Stasiuk, M., Moreno, H., Ablay, G., 1992. Morphological, structural and textural variations in the 1988–1990 andesite lava of Lonquimay Volcano, Chile. Geol. Mag. 129, 657–678.

Pieri, D.C., Baloga, S.M., 1986. Eruption rate, area, and length relationships for some Hawaiian lava flows. J. Volcanol. Geotherm. Res. 30, 29–45.

Proietti, C., Coltelli, M., Marsella, M., Fujita, E., 2009. A quantitative approach for evaluating lava flow simulation reliability: LavaSIM code applied to the 2001 Etna eruption. Geochem. Geophys. Geosyst. 10.

Realmuto, V., Hon, K., Kahle, A., Abbott, E., Pieri, D., 1992. Multispectral thermal infrared mapping of the 1 October 1988 Kupaianaha flow field, Kilauea volcano, Hawaii. Bull. Volcanol. 55, 33–44.

Robertson, J., Kerr, R., 2012. Solidification dynamics in channeled viscoplastic lava flows. J. Geophys. Res., Solid Earth 117, 1978–2012.

Rowland, S., Garbeil, H., Harris, A., 2005. Lengths and hazards from channel-fed lava flows on Mauna Loa, Hawai'i, determined from thermal and downslope modeling with FLOWGO. Bull. Volcanol. 67, 634–647.

Scandone, R., Giacomelli, L., Gasparini, P., 1993. Mount Vesuvius: 2000 years of volcanological observations. J. Volcanol. Geotherm. Res. 58, 5–25.

Self, S., Thordarson, T., Keszthelyi, L., Walker, G., Hon, K., Murphy, M., Long, P., Finnemore, S., 1996. A new model for the emplacement of Columbia River basalts as large, inflated pahoehoe lava flow fields. Geophys. Res. Lett. 23, 2689–2692.

Soule, S., Cashman, K., 2004. The mechanical properties of solidified polyethylene glycol 600, an analog for lava crust. J. Volcanol. Geotherm. Res. 129, 139–153.

Stasiuk, M., Jaupart, C., Sparks, R., 1993. Influence of cooling on lava-flow dynamics. Geology 21, 335–338.

Staudacher, T., Ferrazzini, V., Peltier, A., Kowalski, P., Boissier, P., Catherine, P., Lauret, F., Massin, F., 2009. The April 2007 eruption and the Dolomieu crater collapse, two major events at Piton de la Fournaise (La Réunion Island, Indian Ocean). J. Volcanol. Geotherm. Res. 184, 126–137.

Sutton, A., Elias, T., Kauahikaua, J., 2003. Lava-effusion rates for the Pu'u'ō'Ō–Kupaianaha eruption derived from SO_2 emissions and very low frequency (VLF) measurements. U.S.G.S. Professional Paper 1676, pp. 137–148.

Tazieff, H., 1977. An exceptional eruption: Mt Nyiragongo, Jan. 10th, 1977. Bull. Volcanol. 40, 189–200.

Thordarson, T., Self, S., 1998. The Roza Member, Columbia River Basalt Group: a gigantic pahoehoe lava flow field formed by endogenous processes? J. Geophys. Res. 103, 27411–27427.

Vicari, A., Hérault, A., Del Negro, C., Coltelli, M., Marsella, M., Proietti, C., 2007. Modeling of the 2001 lava flow at Etna volcano by a Cellular Automata approach. Environ. Model. Softw. 22, 1465–1471.

Wadge, G., 1978. Effusion rate and the shape of aa lava flow-fields on Mount Etna. Geology 6, 503–506.

Walker, G., 1973. Lengths of Lava Flows. Philos. Trans. R. Soc. Lond. Ser. A, Math. Phys. Sci. 274, 107–116.

Wright, R., Blake, S., Harris, A., Rothery, D., 2001. A simple explanation for the space-based calculation of lava eruption rates. Earth Planet. Sci. Lett. 192, 223–233.

Wright, R., Flynn, L., Garbeil, H., Harris, A., Pilger, E., 2004. MODVOLC: near-real-time thermal monitoring of global volcanism. J. Volcanol. Geotherm. Res. 135, 29–49.

Wright, R., Garbeil, H., Davies, A., 2010. Cooling rate of some active lavas determined using an orbital imaging spectrometer. J. Geophys. Res. 115, B06205.